ANALYSIS AND DESIGN OF ELECTROTHERMAL ACTUATORS FABRICATED FROM SINGLE CRYSTAL SILICON

John M. Maloney, Don L. DeVoe, David S. Schreiber

Center for Micro Engineering
Department of Mechanical Engineering
and Institute for Systems Research
University of Maryland, College Park

ABSTRACT

Thermal actuators that deflect laterally by resistive heating have been fabricated in single crystal silicon (SCS) by deep reactive ion etching (DRIE). With heights of 50 μm, these high-aspect actuators produce significantly larger forces than similar polysilicon devices. Problems with stiction are also avoided through the use of silicon-on-insulator (SOI) technology. An analytical model is applied to U-beam and V-beam actuator shapes fabricated on SOI wafers. The electrothermal component of the analysis uses an axial conduction model to predict temperature distribution; the thermomechanical component employs elastic beam theory to calculate deflection due to thermal strain. Experimental results are compared to analytical predictions. Deflections of 29 μm for a 1200 μm long, 12 μm wide V-beam actuator were observed, corresponding to a predicted force of 7.6 mN.

INTRODUCTION

In the last decade, electrothermal actuation has begun to receive attention as a viable method for actuating microelectromechanical systems (MEMS). With relatively low voltage requirements and high force output, electrothermal actuation has important advantages over traditional electrostatic actuation [1]. Both in-plane and out-of-plane actuators have been developed that rely on thermal expansion due to resistive heating. Thermal bimorphs [2], buckling beams [3], and compliant structures [4] have all been demonstrated. Additionally, applications such as grippers [5], "elevators" [3], and linear and rotational motors [1,6,7] have been described. Recently, work has been reported on the development of accurate models to predict actuator behavior [8, 9]. The in-plane thermal actuator configurations most frequently modeled fall into two classes: U-beam and V-beam. The U-beam actuator is illustrated in Figure 1. In this structure, deflection occurs from asymmetric heating caused by the unequal widths of the arms. Current flux is higher in the thinner beam, resulting in higher temperature and greater thermal expansion. The flexure increases flexibility in the direction of motion. The V-beam configuration, shown in Figure 2, deflects laterally from thermal expansion of a clamped-clamped beam undergoing uniform heat generation. The beam is offset slightly in the middle to control the direction of deflection.

Past research efforts have focused primarily on polysilicon and electroplated nickel as structural components for thermal actuators. Surface micromachining processes such as MUMPs™ [10] allow complex designs to be fabricated using several layers. However, maximum actuator height in these processes is limited to 2 or 3 μm, the height of the released polysilicon layer(s). This limit constrains actuator forces and can result in stiction problems after release because the devices are relatively compliant perpendicular to the substrate.

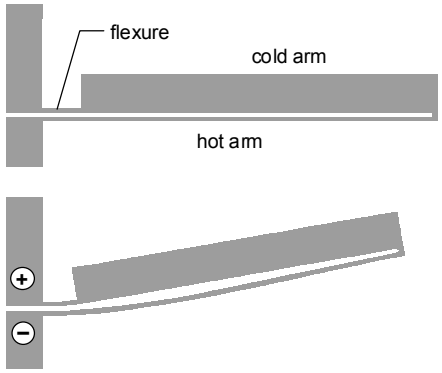

Figure 1. U-beam actuator as fabricated and in operation.

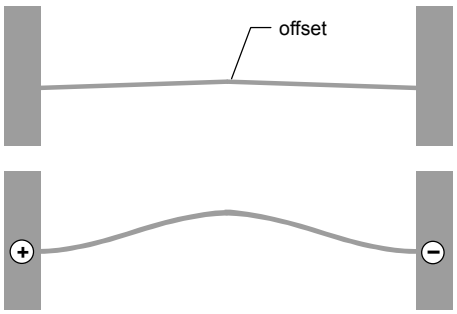

Figure 2. V-beam actuator as fabricated and in operation.

Table 1. Parameters of Theoretical Model.

Parameter	Value
Thermal conductivity, silicon (k_s)	22–148 W m^{-1} K^{-1}
Thermal conductivity, air (k_a)	0.026 W m^{-1} K^{-1}
Resistivity, silicon (ρ)	0.023 Ω-cm
Thermal expansion coefficient (α)	2.51–4.56 x 10^{-6} K^{-1}
Height of beams (h)	50 µm
Gap between beams and substrate (g)	2 µm
Substrate / ambient temperature (T_∞)	293 K

Stiction and bowing have been shown to be a problem with long polysilicon U-beam actuators, limiting their maximum useful length [1]. While LIGA devices avoid these difficulties, the nickel structural material is limited to a maximum temperature of about 450°C [7].

The SCS electrothermal actuators discussed in this paper were fabricated with a single etch of an SOI wafer. This type of fabrication results in advantages over surface micromachining processes. First, bulk micromachining of SCS allows very high aspect ratio devices to be constructed, which in turn allows high forces to be generated, as lateral force scales linearly with height. Second, the larger height results in larger device stiffness perpendicular to the substrate, reducing the possibility of stiction and bowing.

Performance results of U-beam and V-beam actuators fabricated in SCS using DRIE are presented in this paper. This research was initiated to study the design of high force actuator arrays capable of generating 10 mN or more of lateral force. A new model for predicting the deflection of V-beam actuators is also described. This model, which employs the flexibility method of virtual work, is similar to a U-beam model developed by Huang and Lee for polysilicon actuators [9]. The complete theoretical analysis includes both electrothermal and thermomechanical components. Because several of the parameters rely strongly on temperature, predicted results consist of upper and lower bounds of deflection. Experimental results from the fabricated actuators are found to lie between these upper and lower bounds.

THEORETICAL MODEL

An analytical model describing the combined electrical, thermal, and mechanical behavior of V-beam actuators, as shown in Figure 2, has been developed. The model can be divided into two sections: electrothermal analysis and thermomechanical analysis. In the electrothermal analysis, the temperature distribution along the actuator beams is found by solving the heat equation from a differential analysis and boundary conditions. The thermomechanical analysis calculates thermal strain from the increase in beam temperatures and employs the method of virtual work to predict deflection.

Electrothermal Analysis

Because the actuator beam lengths are substantially longer than actuator beam height or widths, a 1-D differential element may be used to model the temperature distribution in the silicon. This element, with height h, width w, and thickness dx, is illustrated in Figure 3. The parameters for this analysis are listed in Table 1; additionally, J represents the current flux through the element. Because of the SOI wafer configuration, the height h of the beams equals the active layer thickness and the gap g between the beams and the substrate equals the oxide layer thickness.

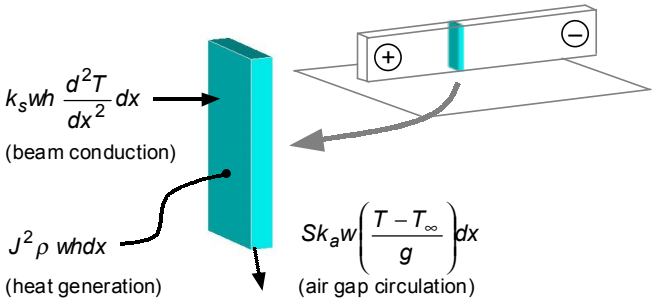

Figure 3. Beam differential element for thermal analysis.

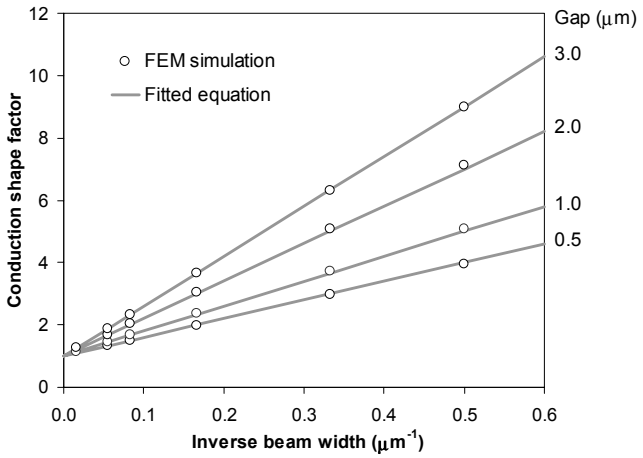

Figure 4. Comparison of conduction shape factor equation and FEM simulation results.

It has been shown that, in the case of a very small gap under a suspended silicon beam, convection and radiation can be considered to be negligible and conduction through air to the substrate dominates [11]. Moreover, conduction from the sides of the beam through the surrounding air to the substrate is not negligible and must be accounted for by the shape conduction factor S [12]. This geometric factor represents the ratio of heat loss from the sides and bottom of the beam to expected heat loss from the bottom of the beam only. An empirical equation has been developed for 2 µm high polysilicon beams [11], but this equation does not scale up well for heights of 50 µm or more. Consequently, it was necessary to develop a new shape factor using finite element modeling, given by

$$S = \frac{4}{w}\left(10^{-6} + g\right) + 1 \qquad (1)$$

This equation was developed by simulating different beam configurations in ANSYS™. Beam widths from 2 to 60 µm and gaps from 0.5 to 3 µm were simulated. Figure 4 compares the fitted equation to simulation results.

Because of the relatively large thickness of the substrate (525 µm), the large 600 x 600 µm anchors, and the high thermal conductivity of SCS, the substrate and anchor temperatures are assumed to be equal to the ambient temperature. The thermal conductivity values of silicon and air are assumed to be independent of temperature to make the differential equation of heat transfer tractable.

Using the differential element in Figure 3, the governing equation of heat transfer can be written as

$$k_s \frac{d^2T(x)}{dx^2} + J^2\rho - Sk_a \frac{T(x)-T_\infty}{gh} = 0 \tag{2}$$

or, by dividing by k_s,

$$\frac{d^2\theta(x)}{dx^2} - m^2\theta(x) = 0 \tag{3}$$

where the following variable substitutions have been made:

$$\theta(x) = T(x) - T_\infty - \frac{J^2\rho}{k_s m^2} \tag{4}$$

$$m^2 = \frac{Sk_a}{k_s gh} \tag{5}$$

The solution to this second-order differential equation is

$$T(x) = T_\infty + \frac{J^2\rho}{k_s m^2} + c_1 e^{mx} + c_2 e^{-mx} \tag{6}$$

This equation describes the temperature distribution for any silicon beam suspended in air and undergoing resistive heating from an applied current. The constants of integration can be determined by applying boundary conditions. For the V-beam actuator, the constants of integration can be found by setting the temperature of both ends of the beam equal to the anchor temperature.

$$T(x)\big|_0 = T(x)\big|_L = T_\infty \tag{7}$$

Similarly, the temperature distribution of the U-beam actuator can be found by solving for the constants of integration; however, as shown in Figure 5, the actuator must be divided into three segments: the hot arm and link, the cold arm, and the flexure. By convention, distances along the U-beam actuator are measured up the hot arm, around the link, and down the cold arm and flexure.

With three segments, there exist three solutions of the above differential equation, each with two constants of integration. However, because the values of temperature and heat flux must be continuous where the segments meet, the boundary condition equations can be written as

$$T_h(x)\big|_0 = T_f(x)\big|_{L_h+L_l+L_c+L_f} = T_\infty \tag{8}$$

$$T_h(x)\big|_{L_h+L_l} = T_c(x)\big|_{L_h+L_l} \tag{9}$$

$$T_c(x)\big|_{L_h+L_l+L_c} = T_f(x)\big|_{L_h+L_l+L_c} \tag{10}$$

$$w_h \frac{dT_h(x)}{dx}\bigg|_{L_h+L_l} = w_c \frac{dT_c(x)}{dx}\bigg|_{L_h+L_l} \tag{11}$$

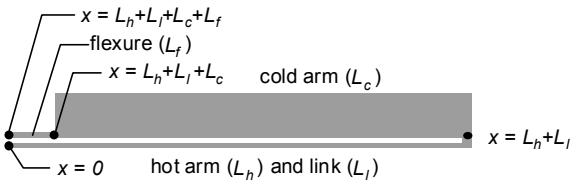

Figure 5. Components of U-beam actuator for electrothermal analysis.

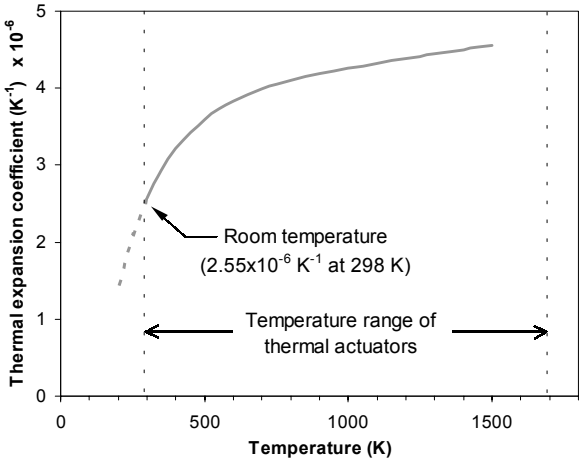

Figure 6. Variation in thermal expansion coefficient with temperature (adapted from [13]).

$$w_c \frac{dT_c(x)}{dx}\bigg|_{L_h+L_l+L_c} = w_f \frac{dT_f(x)}{dx}\bigg|_{L_h+L_l+L_c} \tag{12}$$

where $T_h(x)$, $T_c(x)$, and $T_f(x)$ are the temperature distributions of the hot arm, cold arm, and flexure, respectively. Linear algebra can be used to solve these equations for the constants of integration.

Thermomechanical Analysis

Once the temperature distribution along the actuator has been calculated, the thermal strain of each segment is found using the coefficient of thermal expansion α. Because of the large temperature range over which the SCS actuators operate, α cannot be assumed to remain constant. Okado and Tokumaru developed the following empirical equation for SCS between 300 and 1500 K [13]:

$$\alpha(T) = \left(3.725\left[1 - \mathrm{e}^{-5.88\times10^{-3}(T-124)}\right] + 5.548\times10^{-4}T\right)\times10^{-6}\ \mathrm{K}^{-1} \tag{13}$$

The relationship between the coefficient of thermal expansion and temperature is shown in Figure 6. The thermal strain of each segment is calculated as

$$\Delta L_i = \int_{L_i} \alpha\left[T_i(x)\right]\left[T_i(x) - T_\infty\right]dx = \alpha\left(\overline{T}_i\right) L_i\left(\overline{T}_i - T_\infty\right) \tag{14}$$

where $\overline{T}_i$ is the average temperature of that segment.

The U-beam and V-beam actuators are statically indeterminate structures; however, the method of virtual work can be used to find the reaction forces and actuator deflection. Using the flexibility method of virtual work, the redundant constraints are released and replaced by two unit forces and one moment in the directions of X_1, X_2, and X_3, as shown in Figure 7 [14].

Linear algebra can then be used to solve the following flexibility equation for X_1, X_2, and X_3, which represent the actual constraint forces and moment at the released end:

$$\begin{bmatrix} f_{11} & f_{12} & f_{13} \\ f_{21} & f_{22} & f_{23} \\ f_{31} & f_{32} & f_{33} \end{bmatrix} \begin{bmatrix} X_1 \\ X_2 \\ X_3 \end{bmatrix} + \begin{bmatrix} f_{01} \\ f_{02} \\ f_{03} \end{bmatrix} = \begin{bmatrix} 0 \\ 0 \\ 0 \end{bmatrix} \tag{15}$$

In this equation, each flexibility coefficient f_{ij} represents the displacement of the released end in the direction of X_i due to a unit virtual force or moment in the direction of X_j, and is calculated using

$$f_{ij} = \sum_{k=1}^{n} \left[\int_{L_k} \frac{m_{kj} m_{ki}}{EI_k} dx + \frac{L_k n_{kj} n_{ki}}{EA_k} \right] \tag{16}$$

where m_{ki} and n_{ki} are the bending moment and the axial force in member k due to a unit value of the redundant constraint X_i [14]. Actuator members are identified by the circled numbers in Figure 7. Additionally, the quantity f_{0i} is the displacement of the released end due to thermal strain in the direction of X_i if the redundant constraints are ignored (making the structure statically determinate). In other words, the cumulative effects of the redundant constraints and the thermal strain must result in zero deflection and zero rotation of the released end, since it is actually fixed.

Huang and Lee have derived thermal strains and flexibility coefficients previously for the U-beam actuator [9]. These expressions are adapted for SCS as

$$f_{01} \cong 0 \qquad f_{02} = \Delta L_c + \Delta L_f - \Delta L_h \qquad f_{03} = 0 \tag{17}$$

$$f_{11} = \frac{L_h^3}{3EI_h} + \frac{L_h^2 L_l}{EI_l} + \frac{L_h^3 - L_f^3}{3EI_c} + \frac{L_f^3}{3EI_f} + \frac{L_l}{EA_l} \tag{18}$$

$$f_{12} = f_{21} = -\frac{L_h L_l^2}{2EI_l} - \frac{L_l (L_h^2 - L_f^2)}{2EI_c} - \frac{L_l L_f^2}{2EI_f} \tag{19}$$

$$f_{13} = f_{31} = -\frac{L_h^2}{2EI_h} - \frac{L_h L_l}{EI_l} - \frac{L_h^2 - L_f^2}{2EI_c} - \frac{L_f^2}{2EI_f} \tag{20}$$

$$f_{22} = \frac{L_l^3}{3EI_l} + \frac{L_l^2 L_c}{EI_c} + \frac{L_l^2 L_f}{EI_f} + \frac{L_h}{EA_h} + \frac{L_c}{EA_c} + \frac{L_f}{EA_f} \tag{21}$$

$$f_{23} = f_{32} = \frac{L_l^2}{2EI_l} + \frac{L_l L_c}{EI_c} + \frac{L_l L_f}{EI_f} \tag{22}$$

$$f_{33} = \frac{L_h}{EI_h} + \frac{L_l}{EI_l} + \frac{L_c}{EI_c} + \frac{L_f}{EI_f} \tag{23}$$

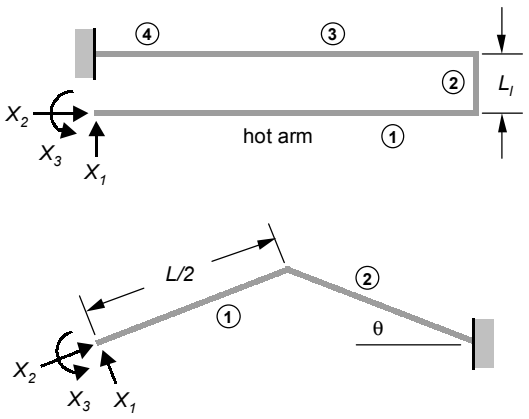

Figure 7. Coordinate systems of U-beam and V-beam actuators for thermomechanical analysis.

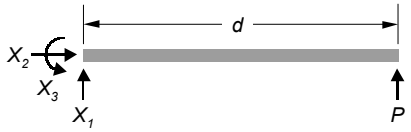

Figure 8. Coordinate system of actuator beam for deflection calculations.

We have derived corresponding expressions for use in modeling V-beam actuators. Because the offset angle of the buckling actuator is typically less than 5 degrees, small angle approximations can be used. Thermal strain produces the following displacements of the released end:

$$f_{01} = \theta \Delta L \qquad f_{02} = -\Delta L \qquad f_{03} = 0 \tag{24}$$

Additionally, the flexibility coefficients of the V-beam actuator are expressed as

$$f_{11} = \frac{L^3}{3EI} + \frac{2L\theta^2}{EA} \tag{25}$$

$$f_{12} = f_{21} = \frac{5L^3\theta}{24EI} - \frac{L\theta}{EA} \tag{26}$$

$$f_{13} = f_{31} = -\frac{L^2}{2EI} \tag{27}$$

$$f_{22} = \frac{L^3\theta^2}{6EI} + \frac{L}{EA} \tag{28}$$

$$f_{23} = f_{32} = -\frac{L^2\theta}{4EI} \tag{29}$$

$$f_{33} = \frac{L}{EI} \tag{30}$$

Once the redundant reaction forces have been found, the actuator deflections are found from Castigliano's theorem [15], which states

that the deflection u of a beam can be expressed as

$$u = \int_0^d \frac{M(x)}{EI} \frac{\partial M(x)}{\partial P} dx \tag{31}$$

where $M(x)$ is the bending moment of the beam and P is a dummy load applied at the desired deflection point, as shown in Figure 8. For the U-beam actuator, the beam represents the hot arm with length L_h; for the V-beam actuator, it represents the left half of the actuator with length $L/2$. Upon integrating and setting P to zero, the deflection at the location of P can be written as

$$u = \frac{d^2}{6EI}\left(X_1 d - 3X_3\right) \tag{32}$$

where X_1 and X_3 are found by solving Equation (15) using the appropriate set of flexibility coefficients.

FABRICATION

U-beam actuators with lengths of 800 μm and V-beam actuators with lengths of 1200 μm were fabricated from an SOI wafer with a heavily-doped 50 μm active layer. The active layer was separated from the wafer substrate by a 2 μm oxide layer. The wafer was patterned with a 5 μm layer of AZ9245 photoresist, and DRIE was used to etch completely through the active layer. After DRIE, the photoresist was removed, and the wafer was diced into several chips. The devices were released by immersing the chips in concentrated hydrofluoric (HF) acid for 12 minutes. The chips were then rinsed with DI water and isopropanol and dried on a hot plate. The actuators moved smoothly under power, and no stiction was observed during operation.

Figures 9 and 10 show scanning electron microscope (SEM) pictures of the fabricated actuators at a magnification of 75x. Vernier scales are connected to the tip of the U-beam actuator and the midpoint of the V-beam actuator to measure deflection. The resolution of these vernier scales is ± 0.5 μm.

DISCUSSION

Variations in the electrical, thermal, and mechanical properties of silicon have a significant effect on actuator performance. As described previously, variations in thermal expansion are readily incorporated into the thermomechanical model once the temperature distribution is known. However, variations in resistivity and thermal conductivity are more difficult to model since they change the linear heat equation given by Equation (2) into a complex nonlinear differential equation with no closed-form solution. The effects of these latter two parameters are discussed here, together with a comparison between modeled performance and experimental results of selected thermal microactuators.

Before the analytical model can be compared to experimental results, the resistivity of the active layer must be determined. This value is entirely dependent on the level of boron doping and cannot be inferred from the properties of SCS. The room temperature resistivity of the wafer used for this research was reported after manufacture to be 0.013 Ω-cm. A four point probe measurement of 0.0133 Ω-cm at our facilities confirmed this value. This resistivity corresponds to a doping level of about 10^{19} atoms/cm^3 for p-type silicon [16]. To further measure resistivity, a probe station was used to apply voltage

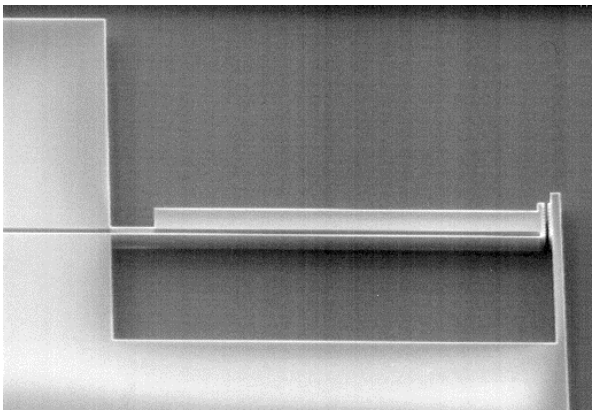

Figure 9. SEM view of an 800 μm long U-beam actuator with an attached vernier scale (75x).

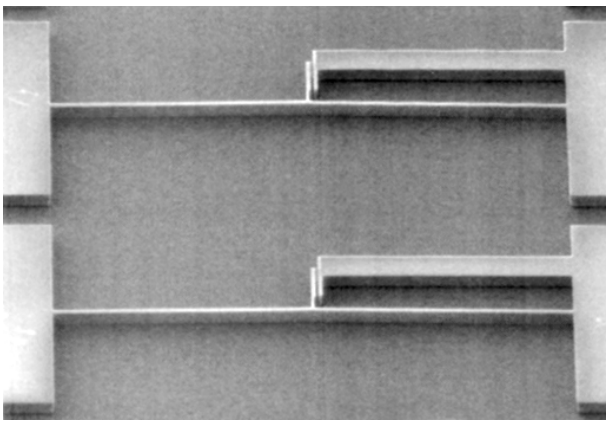

Figure 10. SEM view of two 1200 μm long V-beam actuators with attached vernier scales (75x).

across and measure current through six 1200 μm long suspended silicon beams. Resistivity was calculated as

$$\rho = \frac{Vwh}{IL} \tag{33}$$

where h = 50 μm, the height of the active layer, and w = 10 or 12 μm, depending on which beam was tested. Initial measurements were taken by contacting the probes against bare silicon; however, a high contact resistance at low power was observed. To improve connectivity and obtain more accurate measurements, a 200 Å Cr / 5000 Å Au layer was evaporated onto selected silicon anchors.

The results from all six beams are shown in Figure 11. This chart can be divided into three sections. In the first regime, contact resistance between the probes and the silicon dominates when contacting bare silicon. A native oxide layer that degrades the electrical connection at low power is believed to cause these large initial resistivity measurements. As power is increased, contact resistance drops rapidly until the inherent silicon resistivity dominates. In the second regime, temperature rises proportionally as power increases and the resistivity exhibits a positive temperature coefficient.

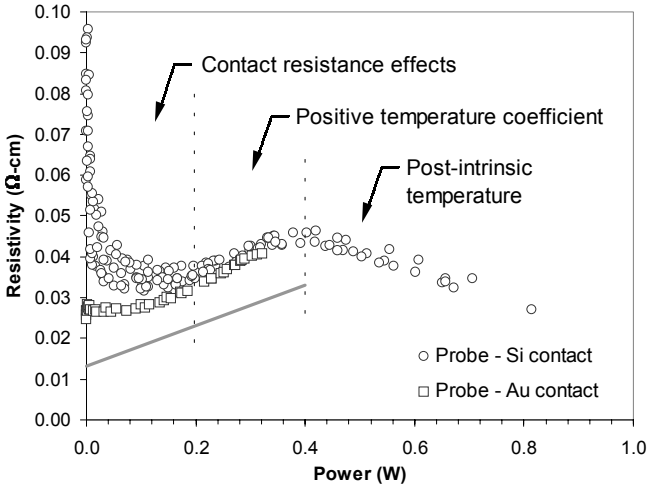

Figure 11. Resistivity vs. applied power for six suspended silicon beams. Solid line represents predicted resistivity.

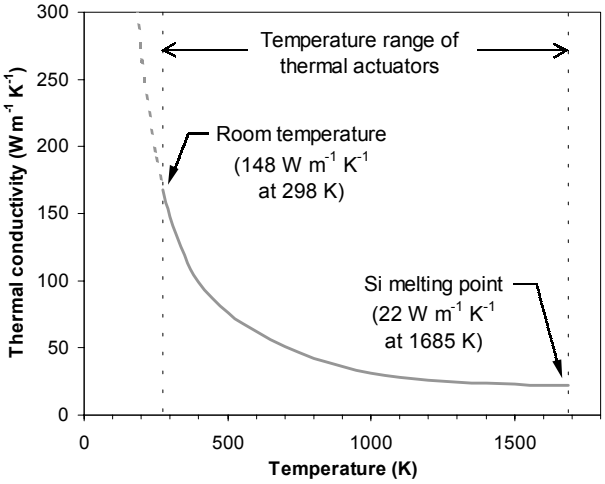

Figure 12. Variation in thermal conductivity with temperature (adapted from [19]).

When the power reaches 0.4 W at a predicted temperature of about 640°C, the resistivity is at a maximum. This behavior has been previously reported in the range of 250–750°C for a doping level around 10^{19} atoms/cm^3 [17,18]. The resistivity peaks at the so-called intrinsic temperature, where intrinsic and dopant charge carriers are equal. In the third regime, the sign of the temperature coefficient of resistivity reverses and resistivity actually decreases with increasing power and temperature.

A line has been drawn in Figure 11 with the slope of the resistivity measurements in the second regime and the intercept of the confirmed room temperature measurement. It is assumed that the resistivity measurements are offset from this line because of a voltage drop across the contact area. A resistivity value of 0.023 Ω-cm, corresponding to the average resistivity between room temperature and the intrinsic temperature, is used for the predicted results presented in this paper. This value is assumed to remain constant with respect to temperature.

As with resistivity, the thermal conductivity of SCS, k_s, exhibits significant variation with temperature [19]. The relationship between temperature and thermal conductivity for the operating range of the SCS thermal actuators is shown in Figure 12. Between room temperature (298 K) and the melting point of silicon (1685 K), the thermal conductivity drops from 148 to 22 W m^{-1} K^{-1}. Although an equation could be fitted to this relationship, the electrothermal solution described above depends on a thermal conductivity that is independent of temperature. However, the range of k_s can be used to provide upper and lower bounds of predicted deflections.

The fabricated actuators were tested by applying current through probes placed in contact with the anchors. Figure 13 shows an example of a V-beam actuator in operation; the vernier scale indicates a deflection of 22 μm with an uncertainty of ± 0.5 μm.

Figure 14 compares predicted and experimental deflections for a U-beam actuator with a 800 μm long, 6 μm wide hot arm; a 720 μm long, 60 μm wide cold arm; a 80 μm long, 6 μm wide flexure; and a link length of 6 μm. Figure 15 compares predicted and experimental deflections for a 1200 μm long, 12 μm wide V-beam actuator with a midpoint offset of 12 μm. In both charts, experimental results are

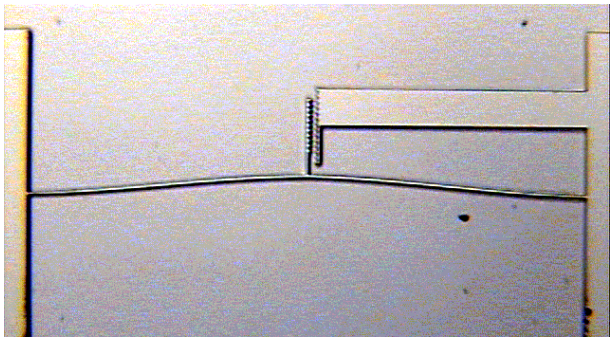

Figure 13. 1200 μm long V-beam actuator in operation.

bounded by predictions using thermal conductivity values of 22 and 148 W m^{-1} K^{-1}. Deflections follow the low-temperature bound of thermal conductivity at low currents and tend towards the high-temperature bound as current rises. This behavior is expected from the temperature-conductivity relationship given in Figure 12. Deflection increases with lower thermal conductivity because heat flow through the beams and anchors to the substrate is reduced. Consequently, higher temperatures can be maintained along actuator beams.

The drop-off in deflection at very high current values is believed to be directly caused by the drop in resistivity when the intrinsic temperature is exceeded in the beam. This effect occurs first at the middle of the beam, where the temperature is highest. As current was increased beyond the intrinsic point during testing, the actuators began to glow until eventually failure by melting was observed.

By FEM simulation using ANSYS, the maximum 35 μm deflection of the U-beam actuator corresponds to a force of 490 μN at the tip. As expected, this force exceeds polysilicon U-beam actuator forces by a factor of over 50 [1]. The maximum 29 μm deflection of the V-beam actuator represents a predicted force of 7.6 mN at the midpoint. Besides exhibiting larger forces, the V-beam actuator has an advantage in its locus of motion. The disadvantage of the U-beam actuator is that translational motion is coupled with rotational motion.

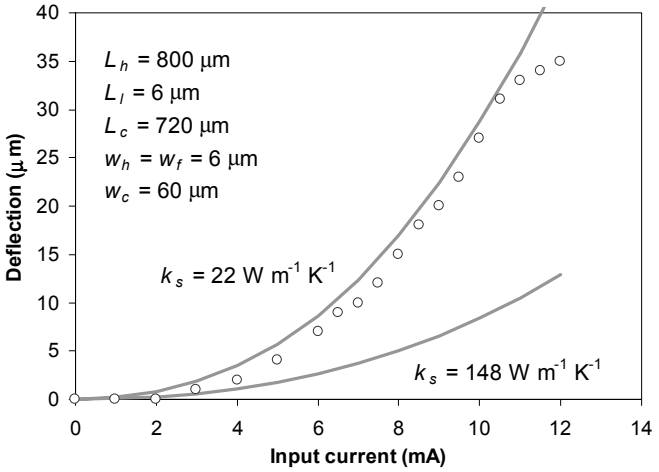

Figure 14. Deflection vs. current for U-beam actuator. Solid lines represents predicted results.

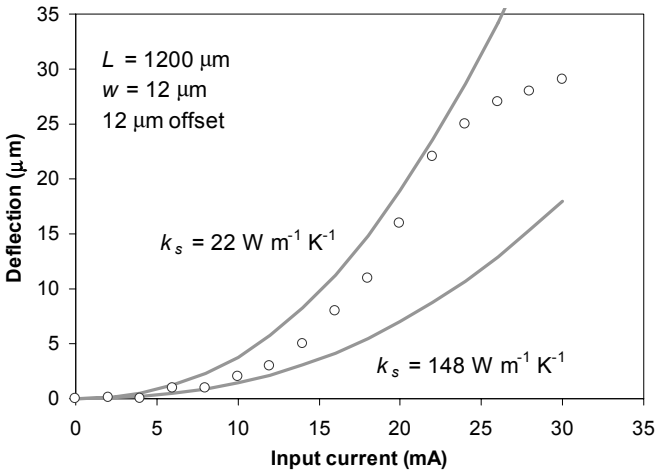

Figure 15. Deflection vs. current for V-beam actuator. Solid lines represents predicted results.

This rotation makes it difficult to connect the ends of the U-beam actuators to produce a high-force array. Although solutions such as pin-slot and rotary-joint yokes have been demonstrated [1], these solutions require a multi-layer process and are not feasible here. However, the V-beam actuator produces only translational motion and is therefore suitable for an array in which the yoke passes through the center of the actuators. When sharing the same two anchors, multiple V-beam actuators would effectively be wired in parallel.

CONCLUSION

U-beam and V-beam thermal actuators have been analyzed using a theoretical model combining electrothermal and thermomechanical components. Displacement equations using virtual work to calculate the deflection of the V-beam actuator have been derived. Actuators have been fabricated on an SOI wafer using DRIE. No stiction or bowing were observed during operation due to the high stiffness of the devices perpendicular to the wafer. Maximum resistivity at an intrinsic temperature point for doped silicon was observed. Experimental deflections of thermal actuators were measured and found to compare well with predicted results. The measured deflection curves were bounded by predicted deflection curves calculated using the upper and lower values of thermal conductivity. These upper and lower values were chosen to correspond to the values of thermal conductivity at highest and lowest actuator temperatures. Variations in silicon resistivity both below and above the intrinsic temperature were observed to have a strong effect on device performance. Similarly, decreased thermal conductivity at high temperatures resulted in larger deflections than predicted by assuming constant material properties. These temperature-dependent variations in the electrical, thermal, and mechanical properties of silicon combine to produce significant displacements and forces for both U-beam and V-beam actuators.

ACKNOWLEDGMENTS

This research was supported under DARPA contract DABT 63-98-10015 and NSF grant DMI 9875817. The authors gratefully acknowledge Mr. Nolan Ballew and Mr. Brett Piekarski for fabrication assistance. DRIE was performed courtesy of the Army Research Laboratory and the Johns Hopkins University Applied Physics Laboratory.

REFERENCES

[1] Comtois, J. H., Michalicek, M. A., and Barron, C. C., 1998, "Electrothermal Actuators Fabricated in Four-Level Planarized Surface Micromachined Polycrystalline Silicon," Sensors and Actuators, **A70**, pp. 23-31.

[2] Riethmüller, W., and Benecke, W., 1988, "Thermally Excited Silicon Microactuators," IEEE Transactions on Electron Devices, **35**, pp. 758-762.

[3] Lin, L., and Lin, S.-H., 1998, "Vertically Driven Microactuators by Electrothermal Buckling Effects," Sensors and Actuators, **A71**, pp. 35-39.

[4] Jonsmann, J., Sigmund, O., and Bouwstra, S., 1999, "Compliant Thermal Microactuators," Sensors and Actuators, **76**, pp. 463-469.

[5] Pan, C. S., and Hsu, W., 1997, "An Electro-Thermally and Laterally Driven Polysilicon Microactuator," Journal of Micromechanics and Microengineering, **7**, pp. 7-13.

[6] Pai, M., and Tien, N. C., 1999, "Current-Controlled Bi-Directional Electrothermally Actuated Vibromotor," Proceedings Transducers 1999 (Sendai, Japan).

[7] Que, L., Park, J.-S., and Gianchandani, Y. B., 1999, "Bent-Beam Electro-Thermal Actuators for High Force Applications," IEEE Conference on Micro Electro Mechanical Systems (Orlando, FL).

[8] Butler, J. T., Bright, V. M., and Cowan, W. D., 1997, "SPICE Modeling of Polysilicon Thermal Actuators," Proceedings SPIE, **3224**, pp. 284-293.

[9] Huang, Q.-A., and Lee, N. K. S., 1999, "Analysis and Design of Polysilicon Thermal Flexure Actuator," Journal of Micromechanics and Microengineering, **9**, pp. 64-70.

[10] Koester, D., Mahedevan, R., and Marcus, K., 1994, "Multi-User MEMS Processes (MUMPs) Introduction and Design Rules," rev. 3, MCNC MEMS Technology Applications Center, http://www.mcnc.org.

[11] Lin, L., and Chiao, M., 1996, "Electrothermal Responses of Lineshape Microstructures," Sensors and Actuators, **A55**, pp. 35-41.

[12] Incropera, F., and DeWitt, D., 1996, *Fundamentals of Heat and Mass Transfer*, John Wiley and Sons, New York.

[13] Okada, Y., and Tokumaru, Y., 1984, "Precise Determination of Lattice Parameter and Thermal Expansion Coefficient of Silicon

Between 300 and 1500 K," Journal of Applied Physics, **56**, pp. 314-320.
[14] Oden, J., 1967, *Mechanics of Elastic Structures*, McGraw-Hill, New York.
[15] Beer, F., and Johnson, E., 1992, *Mechanics of Materials*, McGraw-Hill, New York.
[16] Jaeger, R. C., 1988, *Introduction to Microelectronic Fabrication*, Addison-Wesley, Massachusetts.
[17] Wolkenberg, A., 1990, "Exact Resistivity Calculation of Heavily Doped Silicon," Physica Status Solidi, **A120**, pp. 567-574.
[18] Pearson, G. L., and Bardeen, J., 1949, "Electrical Properties of Pure Silicon and Silicon Alloys Containing Boron and Phosphorous," Physical Review, p. 1.
[19] Touloukian, Y. S., Powell, R. W., Ho, C. Y., and Klemens, P. G., 1970, *Thermophysical Properties of Matter*, IFI/Plenum, New York.